Band mixing in semiconductor superlattices

J. N. Schulman*
Department of Physics and Astronomy, University of Hawaii at Manoa, Honolulu, Hawaii 96822

Yia-Chung Chang
Department of Physics and Materials Research Laboratory, University of Illinois at Urbana—Champaign 1110 West Green Street, Urbana, Illinois 61801

(Received 2 July 1984)

Much understanding of the electronic and optical properties of a semiconductor superlattice can be obtained by relating the superlattice electronic wave functions and band structure to those of the two bulk semiconductors from which it is constructed. In this paper, the relationship is studied within the framework of the empirical tight-binding model, which is solved using the reduced Hamiltonian technique. The superlattice wave functions are described as linear combinations of bulk Bloch functions with complex wave vectors, twenty (including spin) for each of the two constituent materials. The bulk Bloch-function composition of the superlattice wave function is studied as a function of layer thickness, alloy composition, and energy. The GaAs-$Ga_{1-x}Al_xAs$ and InAs-GaSb superlattices are examined in detail. Comparisons with simpler Kronig-Penney and envelope-function models are made. It is found that the lowest superlattice conduction-band states are primarily derived from the expected bulk states with wave vectors near the center of the Brillouin zone, with a small admixture of zone-edge components. The energies and general form of the wave functions are modified only slightly, except close to the interfaces. There, the admixture can significantly affect the interfacial boundary conditions beyond those employed by commonly used envelope-function approximations. Valence-band states are more complicated in that the superlattice periodic potential mixes the bulk heavy-hole, light-hole, and spin-orbit split-off bands, even at the superlattice Brillouin-zone center. Crossover effects occur in which a given superlattice subband can have a varying proportion of light-hole-like or heavy-hole-like character depending on superlattice layer thickness. The dispersion of the subbands away from the zone center also causes the mixing of bands and results in modifications of the superlattice band structure as compared with band structures produced by simpler models.

I. INTRODUCTION

Semiconductor superlattices consist of alternating layers of materials whose electronic properties in themselves are relatively well known. Familiar examples are the GaAs-$Ga_{1-x}Al_xAs$, InAs-GaSb, and CdTe-HgTe superlattices. Theoretical calculations of superlattice electronic properties commonly use some of the bulk information as inputs.[1] For example, the superlattice tight-binding calculations use empirical matrix elements determined by fitting to bulk band structures.[2] Similarly, the various envelope-function methods use bulk effective masses, band gaps, and momentum matrix elements.[3–5]

Despite the use of the bulk information, the results of the superlattice calculations—energy bands and wave functions—are not always easily interpreted in terms of the bulk properties. The concept of zone folding represents perhaps the simplest point of view relating superlattice and bulk band structures.[1] It provides little quantitative information, however.

The envelope-function approximation method is a useful method that is simple enough so that the relationship between the superlattice and bulk wave functions is easily extracted. In fact, the superlattice wave function is written as a linear combination of Brillouin zone-center bulk states with a slowly varying envelope modification along the superlattice axis. The method is adequate for a superlattice state whose energy is in close proximity to a band edge of one of the bulk materials and if only one or two bulk states in each material are expected to dominate.

There are important situations, however, where a more complete description than can be provided by the envelope-function approximation is necessary to obtain an understanding of the superlattice electronic properties. This can occur when two or more bulk states with widely separated wave vectors contribute significantly to a given superlattice state. An example occurs in the superlattice subbands above the lowest conduction subband in the GaAs-$Ga_{1-x}Al_xAs$ superlattice. As the subband energies approach the GaAs X-point conduction-band minimum energy, the superlattice state becomes a mixture of Brillouin-zone-center (Γ-point) and X-point—related bulk states.[6] Since the envelope-function method is based on bulk zone-center states only, the X-point contribution is omitted.

A second example can occur in superlattice valence bands. The envelope-function approximation allows no mixing of bulk heavy- and light-hole states in the superlattice wave function at the superlattice Brillouin-zone center.[4,5] This approximation is realistic if the superlattice heavy- and light-hole-like states are sufficiently separated in energy. As will be shown, however, their en-

ergies are close for certain superlattice layer thicknesses. The light- and heavy-hole mixing has a substantial effect on optical properties.[7] The light- and heavy-hole subbands also mix away from the zone center due to their differing effective masses. The envelope-function method does not account for this for wave vectors parallel to the superlattice axis.

The HgTe-CdTe superlattice provides a related example, in which the heavy hole and conduction bands mix.[8] The envelope-function method predicts that this superlattice is a zero-gap semiconductor for superlattices with HgTe to CdTe layer thickness ratios greater than 5.3 (assuming a zero valence-band discontinuity between the two bulk materials).[4] The zero gap is due to the degeneracy of the first conduction subband and the first heavy-hole subband in this model. The degeneracy is actually caused by the simplicity of the model, however, which omits the mixing of the heavy hole and conduction bands. Including the mixing causes a splitting of the degeneracy, and produces a band gap on the order of that typical of useful HgCdTe alloys with large mercury concentrations. In terms of a group-theoretical analysis, one can say that there are only two zone-center irreducible representations of the HgTe-CdTe superlattice space group, each two dimensional (including spin).[9] The four-dimensional representation predicted by the envelope-function method must, therefore, be split by the conduction—heavy-hole mixing.

In an attempt to more fully explore the relationship between superlattice and bulk electronic properties, we have used the empirical tight-binding model. It has the advantage of incorporating several bulk bands (20 including spin) simultaneously over the full Brillouin zone. The tight-binding model describes the wave function, bulk or superlattice, as a linear combination of atomiclike orbitals. Until recently, the atomic-orbital representation made it difficult to analyze a wave function of a superlattice or, in general, any system involving interfaces, in terms of bulk states, although some progress had been made in specific models.[10,11]

We have developed a new method for solving the tight-binding model which explicitly reveals the bulk-state components of the superlattice wave function. It utilizes a new technique for obtaining the complex bulk band structures—energy as a function of complex wave vector—from an eigenvalue equation. As will be described in the next section, this greatly facilitates solving the superlattice tight-binding equations. An added feature is that the superlattice tight-binding Hamiltonian now has the same dimension for superlattices of arbitrary layer thicknesses, in common with the envelope-function method. An earlier version of the method was used to calculate GaAs-AlAs superlattice conduction-subband dispersion curves in comparison with those obtained from two-band and Kronig-Penney models.[6]

The more complete atomistic description provided by the tight-binding method avoids the previously mentioned oversimplifications which can occur in the envelope-function method.[12] Since the full space group of the superlattice is automatically included, results consistent with group theory must be obtained. For example, the mixing of the bulk heavy-hole and light-hole states in (001) zinc-blende superlattice Brillouin-zone states is clearly allowed. This is because the bulk states that mix are not zone-center states, as in the envelope-function approximation, but have finite wave vectors along the [001] direction. Since all such bulk states have the same symmetry, Δ_5,[13] they can mix in the superlattice wave function.

The details of our calculational technique are given in Sec. II. Section III describes our findings for GaAs-$Ga_{1-x}Al_xAs$ (001) superlattices and Sec. IV for the InAs-GaSb (001) superlattice. The implications of these results for interband optical transitions are described elsewhere.[7]

II. METHOD

The method used to solve the tight-binding equations for the superlattice is a specific application of the reduced Hamiltonian method described elsewhere.[14] It represents a slight improvement over the method used in Ref. 6 in that a smaller Hamiltonian matrix is used. It should be emphasized that the method results in an exact solution within the tight-binding model.

The method is designed to find the energy and wave function of one superlattice state at a time, specified by a given wave vector perpendicular to the superlattice axis, $\mathbf{k}_t$, and wave vector parallel to its axis, k_z. An initial guess for the energy of the state must be made. Then, all of the bulk states with that energy and the given $\mathbf{k}_t$ in both constituent materials of the superlattice are found. Each bulk state can be specified by q_i, its complex wave vector in the z direction. The q_i and the bulk states, ψ_i, are found by diagonalizing a simple matrix constructed from the bulk tight-binding Hamiltonians as described in Ref. 14. Note that k_z, the superlattice wave vector in the z direction, is not the same as any of the bulk wave vectors, q_i, used in constructing the superlattice wave function.

The purely real q_i are the ordinary real wave vectors of the bulk Bloch states. The q_i with nonzero imaginary parts are the wave vectors for evanescent solutions which decay away from each superlattice interface in either direction. The inverse of the imaginary part of q_i is the exponential decay length of the state. The number of q_i depends on the number of orbitals per atom included, the number of nearest-neighbor overlaps included, and the orientation of the superlattice layers. For the (001) zinc-blende superlattices considered here we use five orbitals per atom (s,x,y,z,s^*) and nearest-neighbor overlaps only.[15] This produces 20 bulk states per material, including spin.

The reduced Hamiltonian method is implemented here by expanding the superlattice wave function as a linear combination of bulk Bloch functions ψ_i^A in the material A layers and ψ_i^B in the B layers:

$$\Psi=\sum_l e^{ik_z ld}\sum_i C_i^{A,B}\psi_i^{A,B}(l)\ . \tag{1}$$

$\mathbf{k}_t$ is implicit in this equation. d is the spacing between superlattice unit cells labeled by the integers l.

Additional orbitals for the interface atoms were unnecessarily included in Ref. 6. The transfer-matrix point of view[14,16] makes clear that the wave function at the interface is already determined if the correct linear combination of bulk states is known. In fact, it is sufficient to include a sum over bulk states on the A or B layers only. The wave function on the other layers can be found using the transfer matrix. For computational convenience, however, both sets of bulk states were used in this study.

The 40 unknown coefficients $C_i^{A,B}$ and energy are then found by diagonalizing the Hamiltonian formed using the $\psi_i^{A,B}$ as a basis. Since an energy is assumed in calculating the bulk states to begin with, this procedure must be iterated until an energy resulting from the matrix diagonalization coincides with the energy assumed.[14] Finally, the wave function can be expressed in terms of local-orbital coefficients using the $C_i^{A,B}$ and the known expressions for the $\psi_i^{A,B}$ in terms of local orbitals.

III. GaAs-$Ga_{1-x}Al_xAs$ (001) SUPERLATTICE

A. Bulk complex band structures

Superlattice states with $\mathbf{k}_t=\mathbf{0}$ will be discussed first. The relevant bulk states also must have $\mathbf{k}_t=\mathbf{0}$. Their wave vectors, q_i, can be identified from Fig. 1. It shows the complex band structures of GaAs, AlAs, and $Ga_{0.7}Al_{0.3}As$ in the [001] direction. The units of q are $2\pi/a$, where a is the conventional zinc-blende unit cell length. The bands with purely real or purely imaginary q are drawn with solid lines in the right and left portions of each graph, respectively. The q with nonzero real and imaginary parts are indicated by pairs of dashed lines, the real part in the right portion and the imaginary part in the left. The zero of energy is the GaAs valence-band maximum. The AlAs parameters are adjusted so that the AlAs valence-band maximum is at -0.236 eV. This corresponds to a valence-band discontinuity of 15% of the direct band-gap difference between GaAs and AlAs.[17] The $Ga_{0.7}Al_{0.3}As$ parameters were weighted averages of the GaAs and AlAs parameters.

Table I lists the values of a few of the more important quantities produced by the empirical tight-binding parameters employed here. The parameters are slightly modified versions of those listed in Ref. 15. They are listed in Table II. They were adjusted in order to more accurately reproduce the energy bands in the vicinity of the valence- and conduction-band edges, especially the effective masses. Note that it was possible to reproduce the experimental values of the conduction-, heavy-hole, light-hole, and split-off-band effective masses with good precision.

The conventional band structures, due to the purely real q, can be clearly seen in the right portion of each graph in Fig. 1. The energy region shown includes the split-off, light-hole, and heavy-hole valence bands and the bottommost conduction band. The GaAs indirect minimum occurs at $q=0.84(2\pi/a)$. The AlAs indirect minimum occurs at $q=0.79(2\pi/a)$.

The energy bands due to complex values of q behave in a well understood manner. A thorough discussion of complex band structures of the zinc-blende semiconductors can be found in Ref. 11. In general, the complex q bands emanate from maxima or minima of the real bands. If an extremum occurs at $q=0$, the real part of q for the complex q band emanating from that extremum is zero. This is the case for the complex q band emanating from the valence-band maxima and the direct conduction-band minima in GaAs and AlAs. If the extrema occurs at the zone boundary, the X point, the real part of q for the complex q band also starts out at the X point and its imaginary part increases from zero. See, for example, the next band above the GaAs or AlAs indirect conduction-band minimum. A complex q band emanating from an extremum at an arbitrary point in the Brillouin zone will have both real and imaginary parts. The band structure near the GaAs or AlAs conduction indirect minimum demonstrates this.

There are 20 bands in each material at each energy, although they are not all shown in Fig. 1. The bands omitted are related to the ones shown by negating and/or complex conjugating q, and by considering both spins. The symmetry along the [001] directions ensures that the omitted bands have the same energies as the ones shown.

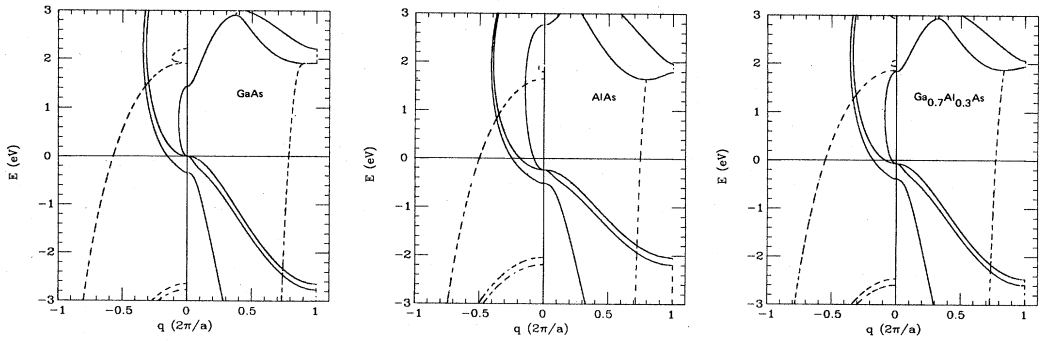

FIG. 1. Band structures of GaAs, AlAs, and $Ga_{0.7}Al_{0.3}As$ in the [001] direction for complex wave vector q. The zero of energy is the GaAs valence-band maximum. The units of q are $2\pi/a$, where a is the conventional lattice constant. Real q is plotted in the right portion of each graph, imaginary q in the left. Bands with purely real or purely imaginary q are represented by solid lines; complex q by pairs of dashed lines.

TABLE I. Bulk effective masses and energy splittings of GaAs, AlAs, $Ga_{0.7}Al_{0.3}As$, InAs, and GaSb produced by the empirical tight-binding method. Energies are in eV. E_{dir} is the direct band gap, E_{ind} is the indirect band gap at or near the X point. E_{SO} is the heavy-hole—split-off band-energy separation. m_C is the zone-center conduction-band effective mass. Effective masses are those in the [001] direction.

	E_{dir}	E_{ind}	E_{SO}	m_C	m_{HH}	m_{LH}	m_{SO}
GaAs	1.430	1.910	0.343	0.067	0.45	0.070	0.14
AlAs	3.002	1.881	0.281	0.22	0.75	0.15	0.27
$Ga_{0.7}Al_{0.3}As$	1.901	1.933	0.324	0.10	0.52	0.093	0.18
InAs	0.410	2.141	0.411	0.023	0.41	0.027	0.094
GaSb	0.810	0.950	0.800	0.049	0.33	0.051	0.155

B. Band mixing

As an example of how the bulk states combine to form the superlattice wave function, it is instructive to analyze a particular superlattice in detail over a large energy range. The GaAs-AlAs (001) superlattice with 17 layers of GaAs (50 Å) and 17 layers of AlAs will be considered here. Table III lists the superlattice-state energies from −0.414 to 1.563 eV at the Brillouin-zone center. The values of the complex wave vectors, q_i, of the eight independent bulk states (four for each material) that contribute to the superlattice state are listed. They are identified as conduction—light-hole (C-LH), heavy-hole (HH), spin-orbit split-off (SO), or X-point states. Since the complex wave-vector bands connect the familiar real bands across band gaps, the labeling of the bands needs clarification. The purely imaginary band emanating from the direct bulk conduction-band minimum connects with the light-hole band. States belonging to this band, the light-hole band, or the conduction band near its minimum are listed under the C-LH column in Table III. The other purely imaginary band emanating from the valence-band maxima is the continuation of the real heavy-hole band. States belonging to it are under the HH column of Table III. Similarly, the imaginary wave-vector band emanating from the split-off band maximum is under the SO column and the complex wave-vector band emanating from the indirect conduction-band minimum at or near the X point is under the X column. The real and imaginary parts of the wave vectors are given in units of $2\pi/a$.

The relative contributions of the various complex wave-vector bulk states to the superlattice wave function can be ascertained from the four columns at the right of the table. There are shown the squares of the amplitudes [the C_i of Eq. (1)] of each of the bulk states. Since complex wave-vector states are not orthonormal,[18] the squared amplitudes do not add to unity, and so they give only an approximate guide to the importance of each bulk state. The bulk states themselves have been normalized so that the sum of the squares of the amplitudes of the orthonormal atomic orbitals add to unity at the origin. In setting up the superlattice Hamiltonian, the layer of arsenic atoms at the interface between the GaAs and AlAs slabs is taken to be the origin. Thus the numbers shown are an approximate measure of the relative influence of the bulk states near the interface.

Table III reveals that one bulk state from each material is dominant in each superlattice state. The superlattice states, therefore, may be labeled according to which bulk state—C-LH, HH, SO, or X—is dominant. In almost all

TABLE II. Empirical tight-binding parameters in eV for GaAs, AlAs, InAs, and GaSb. Notation is that of Refs. 26 and 27. The GaAs and InSb parameters in the two right columns are used at the InAs-GaSb interfaces.

Parameter	GaAs	AlAs	InAs	GaSb	GaAs	InSb
$E_{ss}(000)_a$	−8.4570	−7.6201	−9.6752	−7.5810		
$E_{pp}(000)_a$	0.9275	0.8905	0.7728	0.5951		
$E_{ss}(000)_c$	−2.7788	−1.1786	−2.7053	−3.7070		
$E_{pp}(000)_c$	3.5547	3.4939	3.5830	2.6543		
$4E_{ss}(\frac{1}{2},\frac{1}{2},\frac{1}{2})$	−6.4513	−6.6642	−5.6052	−6.1567	−6.4513	−5.5193
$4E_{xx}(\frac{1}{2},\frac{1}{2},\frac{1}{2})$	1.9546	1.8780	1.8398	1.5789	1.9546	1.4018
$4E_{xy}(\frac{1}{2},\frac{1}{2},\frac{1}{2})$	4.7700	3.8600	4.5492	4.4500	5.0779	3.8761
$4E_{sx}(\frac{1}{2},\frac{1}{2},\frac{1}{2})_{ac}$	4.4800	5.1106	3.0354	4.9601	4.4800	3.7880
$4E_{sx}(\frac{1}{2},\frac{1}{2},\frac{1}{2})_{ca}$	7.8500	6.3000	6.9000	6.4500	5.7839	4.5900
$E_{s^*s^*}(000)_a$	8.4775	7.3905	7.2720	6.3751		
$E_{s^*s^*}(000)_c$	6.6247	6.6339	6.6030	5.7243		
$4E_{s^*x}(\frac{1}{2},\frac{1}{2},\frac{1}{2})_{ac}$	4.8422	4.5216	3.3744	4.9895	4.8422	3.5666
$4E_{x^*x}(\frac{1}{2},\frac{1}{2},\frac{1}{2})_{ca}$	7.0000	7.2000	3.9097	4.2180	4.8077	3.4048
Δ_a	0.3900	0.3500	0.4160	0.9720		
Δ_c	0.1740	0.0240	0.3920	0.1740		

TABLE III. Energies of zone-center states of the GaAs-AlAs (001) superlattice with 17 alternating layers of GaAs and AlAs. The complex wave vectors and squared amplitudes of the bulk GaAs and AlAs conduction-, light-hole-, heavy-hole-, split-off-, and X-point-derived components are shown. Energy is in eV. The GaAs valence-band maximum is the zero of energy.

	Wave vector ($2\pi/a$)				Squared amplitude (10^{-3})			
Energy	C-LH	HH	SO	X	C-LH	HH	SO	X
				GaAs				
1.563	(0.046,0)	(0,0.303)	(0,0.331)	(0.840,0.284)	23.5	0.0	0.0	0.2
−0.021	(0.018,0)	(0.045,0)	(0,0.148)	(0.784,0.576)	0.0	22.5	0.3	0.0
−0.057	(0.031,0)	(0.075,0)	(0,0.137)	(0.783,0.581)	16.0	1.1	0.5	0.0
−0.083	(0.038,0)	(0.091,0)	(0,0.128)	(0.782,0.584)	1.2	21.1	1.8	0.0
−0.169	(0.061,0)	(0.131,0)	(0,0.097)	(0.780,0.593)	2.0	18.0	0.7	0.0
−0.219	(0.076,0)	(0.150,0)	(0,0.076)	(0.779,0.598)	22.7	2.4	8.3	0.0
−0.260	(0.091,0)	(0.165,0)	(0,0.058)	(0.778,0.603)	0.0	2.3	0.1	0.0
−0.268	(0.094,0)	(0.167,0)	(0,0.054)	(0.778,0.604)	2.1	12.0	0.0	0.0
−0.287	(0.102,0)	(0.174,0)	(0,0.045)	(0.778,0.606)	6.7	0.6	9.1	0.0
−0.351	(0.126,0)	(0.194,0)	(0.015,0)	(0.776,0.612)	2.3	6.8	0.4	0.0
−0.385	(0.139,0)	(0.204,0)	(0.034,0)	(0.775,0.616)	0.6	8.9	0.0	0.0
−0.386	(0.140,0)	(0.205,0)	(0.034,0)	(0.775,0.616)	10.7	1.7	3.1	0.0
−0.397	(0.144,0)	(0.208,0)	(0.038,0)	(0.775,0.617)	4.1	2.1	11.5	0.0
−0.414	(0.150,0)	(0.213,0)	(0.043,0)	(0.775,0.619)	8.9	0.0	3.1	0.0
				AlAs				
1.563	(0,0.148)	(0,0.390)	(0,0.407)	(0.787,0.123)	13.9	0.0	0.0	0.2
−0.021	(0,0.075)	(0,0.178)	(0,0.243)	(0.749,0.503)	0.0	13.3	0.2	0.0
−0.057	(0,0.069)	(0,0.164)	(0,0.234)	(0.748,0.508)	19.6	3.6	2.1	0.0
−0.083	(0,0.065)	(0,0.152)	(0,0.227)	(0.747,0.511)	0.9	40.8	0.5	0.0
−0.169	(0,0.044)	(0,0.102)	(0,0.201)	(0.746,0.521)	3.2	64.1	5.8	0.0
−0.219	(0,0.023)	(0,0.052)	(0,0.183)	(0.745,0.527)	47.1	4.1	6.8	0.0
−0.260	(0.028,0)	(0.062,0)	(0,0.167)	(0.744,0.532)	0.0	28.3	0.0	0.0
−0.268	(0.033,0)	(0.072,0)	(0,0.164)	(0.744,0.533)	0.5	12.6	4.5	0.0
−0.287	(0.042,0)	(0.091,0)	(0,0.156)	(0.744,0.535)	13.9	1.4	0.3	0.0
−0.351	(0.068,0)	(0.138,0)	(0,0.126)	(0.743,0.542)	1.4	18.9	11.5	0.0
−0.385	(0.081,0)	(0.158,0)	(0,0.107)	(0.742,0.546)	0.0	18.7	1.1	0.0
−0.386	(0.082,0)	(0.159,0)	(0,0.107)	(0.742,0.546)	13.6	1.2	0.0	0.0
−0.397	(0.086,0)	(0.165,0)	(0,0.101)	(0.742,0.547)	0.3	1.2	43.8	0.0
−0.414	(0.094,0)	(0.174,0)	(0,0.091)	(0.742,0.549)	17.4	0.6	5.7	0.0

cases shown, the same bulk state is dominant in each material. The exception is the state with energy −0.287 eV. The light-hole bulk state has the largest squared amplitude in the AlAs layers, 13.9×10^{-3}, and the split-off component is largest in the GaAs, 9.1×10^{-3} for this state. However, the table also shows that the wave vector of the GaAs split-off state is imaginary at this energy. Its imaginary part cuts the contribution from the state off more than a few layers away from the interface, thus leaving the light-hole state with its real wave vector to dominate. In effect, therefore, this superlattice state can be classified as light-hole-like.

The AlAs valence-band maximum is at an energy of −0.236 eV. The superlattice states with energies of −0.260 eV and below in Table III are therefore not necessarily confined in the GaAs layers. Spatial plots of these states show that the amplitudes are significant in both the GaAs and AlAs layers. An example is shown in Fig. 2 for the −0.260 eV state. This is the first unconfined heavy-hole state. Its form is similar to that of the wave function produced by the Kronig-Penney model, showing that this "antiwell" state is not an artifact of the tight-binding model used here. If the GaAs layer thickness were imagined to increase to infinity with the AlAs layer thickness fixed, this state would become a resonant scattering state with enhanced amplitude on the AlAs layers.

Antiwell states may have important implications for

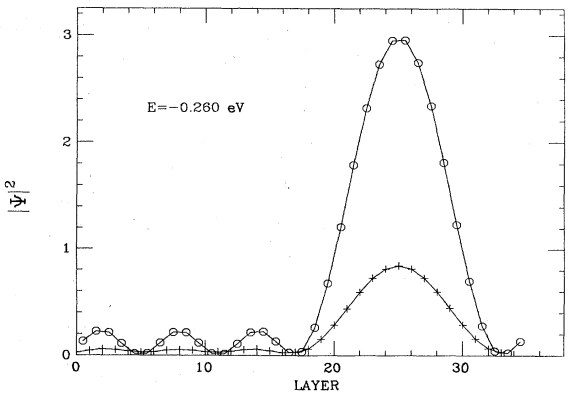

FIG. 2. Tight-binding wave function for the GaAs-AlAs (001) superlattice with 17 alternating layers of GaAs and AlAs with energy −0.260 eV. Open circles indicate anion squared amplitudes and + 's indicate cation squared amplitudes. The first 17 layers are GaAs and the second 17 layers are AlAs.

type-2 superlattices, where the conduction electrons are confined in one type of layer and the valence holes in the other. The separation of the charge carriers would ordinarily reduce the intensity of optical transitions. Transitions between antiwell valence states and ordinary conduction states would not be so reduced, because the confinement is again in the same layers.

The only state with energy below -0.236 eV in Table III which is still mostly confined to the GaAs layers is the one with energy -0.397 eV. This is the first superlattice state with mostly spin-orbit split-off band character. This is due to a small 0.174 eV discontinuity between the GaAs and AlAs split-off valence-band maximum energies. The decay into the AlAs layers is small despite the fact that the heavy-hole and light-hole bulk wave vectors are real at this energy (Table III).

C. Comparison with Kronig-Penney model

Since the superlattice states are dominated by just one bulk state each, it may be conjectured that there is a one-to-one correspondence between these states and superlattice states as calculated using a one-band Kronig-Penney model for the superlattice. Table IV confirms that this is the case here. It lists the superlattice energies as calculated using the tight-binding model (from Table III) and using the Kronig-Penney model. The Kronig-Penney model was applied separately for the direct conduction, heavy-hole, light-hole, and split-off bands using the effective masses from Table I and barrier heights deduced from the energy splittings given in Table I.

Agreement between the Kronig-Penney and tight-binding results is best for the heavy-hole energies. The two methods disagree by less than a millivolt for the top two energies, -0.021 and -0.083 eV. The results for the third energy disagree by about 10 meV. Agreement improves for the fourth subband, but worsens for the lower ones.

The reason for the good agreement for the heavy-hole energies is the high degree of parabolicity of the bulk heavy-hole bands. This is illustrated in Fig. 3 which expands the band structure near $q=0$ of Fig. 1 and plots the bulk energies versus q^2 for GaAs, AlAs, and $Ga_{0.7}Al_{0.3}As$. The bands have been shifted in energy so that their $q=0$ energies are all zero. The conduction (dotted, heavy-hole (dashed), light-hole (dashed-dotted), and split-off (solid) bands are shown. The perfectly parabolic dispersion curves of the effective-mass model are also shown using the same line types. The effective masses of Table I were used for them. The heavy-hole band is seen to be the closest to parabolic, resulting in the

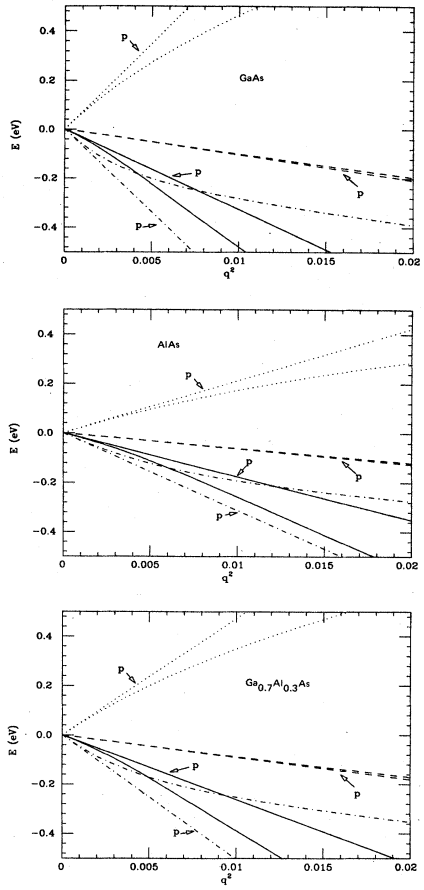

FIG. 3. Band structures of GaAs, AlAs, and $Ga_{0.7}Al_{0.3}As$ in the [001] direction versus q^2. Each band is shifted in energy so that its energy is zero at the Brillouin zone center. Dotted line: conduction band. Dashed line: heavy-hole band. Dashed-dotted line: light-hole band. Solid line: split-off band. Straight lines indicate perfectly parabolic bands (p). The units of q are $2\pi/a$.

TABLE IV. Comparison of zone-center GaAs-AlAs (001) superlattice state energies as calculated by the tight-binding (TB) and one-band Kronig-Penney (KP) models. The superlattice consists of 17 alternating layers of GaAs and AlAs, as in Table III. Energies are in eV. All energies are given relative to the edges of their respective wells.

Conduction		Heavy hole		Light hole		Split-off	
KP	TB	KP	TB	KP	TB	KP	TB
0.112	0.133	−0.021	−0.21	−0.064	−0.057	−0.039	−0.054
		− 0.083	−0.083	−0.283	−0.219		
		−0.182	−0.169	−0.329	−0.287		
		−0.261	−0.260		−0.386		
		−0.284	−0.268				
		−0.377	−0.351				
		−0.406	−0.385				

good agreement between the tight-binding and Kronig-Penney energies.

The improvement in agreement just noted for the fourth heavy-hole band energy is easily explained. As discussed in the Sec. III B, the fourth subband is the first one whose energy is below the AlAs valence-band maximum and it is thus localized in the AlAs layers. Since its energy, -0.260 eV, is close to the AlAs valence-band edge, -0.236 eV, the AlAs heavy-hole band is still nearly parabolic and thus agrees well with the Kronig-Penney result. The lower heavy-hole states also are mostly on the AlAs layers, but their energies are further from the AlAs valence-band edge with the resulting discrepancies seen in Table IV.

The bulk conduction, light-hole, and split-off bands are all substantially less parabolic than the heavy-hole band, as can be seen in Fig. 3. The superlattice energies as determined by the tight-binding and Kronig-Penney models are correspondingly in agreement less. Table III shows that another contribution to the discrepancy is that the superlattice states in these bands are less purely constructed from just one bulk component as compared with the heavy-hole derived states. The relative importance of the two effects varies from state to state.

The Kronig-Penney model is a better approximation for obtaining the energies of the high-lying valence-band states of superlattices with larger GaAs layer thicknesses or with the $Ga_{1-x}Al_xAs$ alloy replacing pure AlAs as the barrier material. This is again because the energies of the states in such superlattices are closer to the GaAs valence-band edge where the bulk bands are parabolic.

D. Subband dispersion

Figure 4 shows the dispersion of the top seven valence subbands of the GaAs-$Ga_{0.7}Al_{0.3}As$ superlattice with 30 GaAs layers (85 Å) alternating with ten alloy layers (28 Å). The dispersion in the z direction is shown. The Kronig-Penney heavy-hole bands are indicated by + 's and the light-hole bands by dashes. Solid lines indicate the tight-binding results.

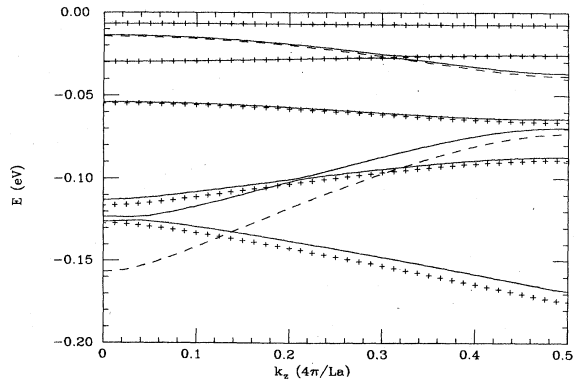

FIG. 4. GaAs-$Ga_{0.7}Al_{0.3}As$ (001) superlattice band structure in k_z direction for 30 GaAs layers alternating with ten alloy layers. Solid lines : tight-binding. + 's: heavy-hole Kronig-Penney model. Dashed lines: light-hole Kronig-Penney model. The zero of energy is the GaAs valence-band maximum. L is the number of layers per unit cell, 40 in this case.

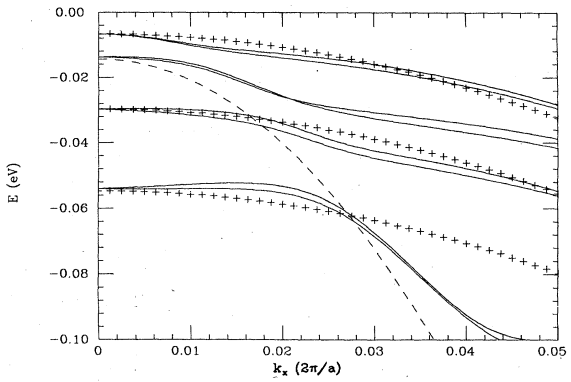

FIG. 5. GaAs-$Ga_{0.7}As_{0.3}As$ (001) superlattice band structure in k_x direction for 30 GaAs layers alternating with ten alloy layers. Solid lines: tight-binding. + 's: heavy-hole Kronig-Penney model. Dashed lines: light-hole Kronig-Penney model. The zero of energy is the GaAs valence-band maximum.

The four highest-energy tight-binding bands are very well reproduced by the three heavy-hole and one light-hole Kronig-Penney bands. Note that the second and third tight-binding subbands do not cross. In general, C_{2v} is the symmetry group along this direction. The only representation of the double group is a single two-dimensional one, and thus all bands are spin-doubly degenerate and do not cross each other.[19] This is also seen for the fifth and sixth subbands, which also do not cross.

Deviations from the Kronig-Penney bands are more noticeable in the three lowest subbands, especially for the lower light-hole band. The bands still agree qualitatively, however. Superlattice states due to the bulk spin-orbit split-off bands are further down in energy.

The dispersion of the superlattice subbands for nonzero $\mathbf{k}_t$ are, not surprisingly, poorly reproduced by the Kronig-Penney model. Figure 5 shows the superlattice band structure in the k_x direction with k_y and k_z equal to zero. The heavy-hole and light-hole Kronig-Penney results are also shown in a manner similar to Fig. 4. In this direction the spin-orbit interaction splits the spin degeneracy causing doubled curves for the tight-binding case. The symmetry group is C_2 which has two one-dimensional representations only.[19,20] The subbands belonging to different representations can cross as can be seen in the figure.

There are three reasons for the failure of the Kronig-Penney model here: the nonparabolicity of the bulk band structure, the mixing of superlattice bands when they are close in energy, and, most importantly, the mixing of light- and heavy-hole character for $\mathbf{k}_t$ not equal to zero. An envelope-function approximation with suitable modifications can include this last effect and should give good agreement with the tight-binding curves.[5]

E. Band-mixing dependence on layer thickness

If $\mathbf{k}_t=0$, the most important deviations from the Kronig-Penney model occur for layer thicknesses and barrier alloy concentrations for which the light- and heavy-hole subbands are close in energy. This can easily occur

away from the Brillouin zone center as seen in Sec. III D. Since optical and transport properties depend mostly on the band structure near the zone center, however, it is of interest to examine the cases where the heavy-hole—light-hole band crossing occurs there.

Consideration of a single quantum well in the effective-mass model implies that the first light hole (LH1) and the second heavy hole (HH2) energies at the zone center should cross as the well thickness is varied, for a given barrier-layer thickness and barrier-alloy composition. As the well thickness is decreased, all states in such a system become unbound except for the $n=1$ heavy-hole (HH1) and light-hole (LH1) states, which are always bound.[21] For large well thicknesses, the energies go as n^2/m, where m is the effective mass. Using the GaAs light-hole and heavy-hole effective masses from Table I it can be seen that the HH2 is more deeply bound than the LH1. Since the opposite is true for small well layer thicknesses, the LH1 and HH2 zone-center state energies must cross.

Figure 6 demonstrates this for the GaAs-$Ga_{0.7}Al_{0.3}As$ superlattice with 20 alloy layers forming the barrier and a varying number of GaAs well layers. The top band is heavy-hole-like for all layer thicknesses. The wave functions for the states in the second band are predominantly light-hole-like, LH1, and the third band down is predominantly heavy hole-like, HH2, for small-well layer thicknesses. Spatial plots of the wave functions in the bands at these layer thicknesses strongly resemble Kronig-Penney plane-wave states.

As the GaAs layer thickness increases, the second and third bands approach each other in energy. The bands attain their closest approach between 65 and 70 GaAs layers, and then separate slightly. They do not actually cross due to the aforementioned symmetry considerations. What does cross is the heavy-hole or light-hole character of the bands. Figure 7 plots the squared amplitudes of the light-hole and heavy-hole bulk states for the second and third bands at the Brillouin zone center as the GaAs layer thickness is varied. The squared amplitudes become equal in the second band state for 67 layers of GaAs. For greater GaAs layer thicknesses, the light-hole component

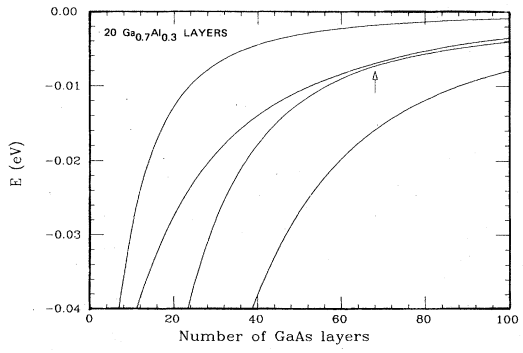

FIG. 6. Brillouin zone-center valence-band energies for the GaAs-$Ga_{0.7}Al_{03}As$ superlattice with 20 alloy layers alternating with a varying number of GaAs layers. The top four bands are shown. The zero of energy is the GaAs valence-band maximum. The arrow indicates the heavy-hole—light-hole crossover thickness.

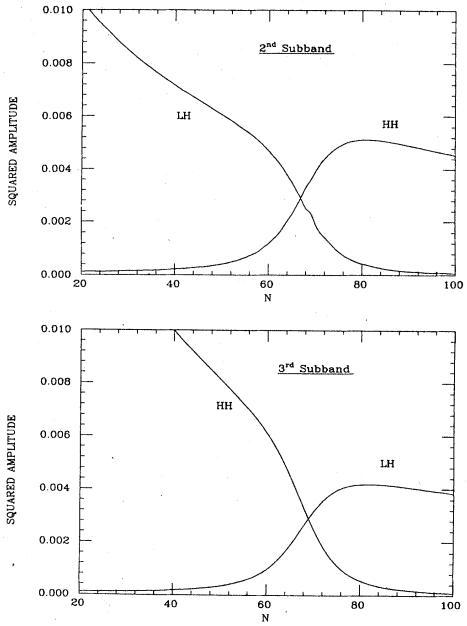

FIG. 7. Squared amplitude of the bulk heavy-hole state and that of the light-hole state in the superlattice wave function for the second and third valence subbands at the Brillouin zone center. The superlattice consists of twenty layers of $Ga_{0.7}Al_{0.3}As$ alternating with N layers of GaAs.

decays to zero and the state becomes heavy-hole-like. The opposite is true for the third band state which switches from heavy hole to light hole in character for more than 68 GaAs layers.

Note that the transition between light-hole and heavy-hole character occurs over about 20 GaAs layers. Even though the effect of this bulk band mixing on the superlattice state energy is small, as seen in Fig. 6, the effect on the wave function is large, and fine tuning of layer thicknesses is not needed in order to observe it. In partic-

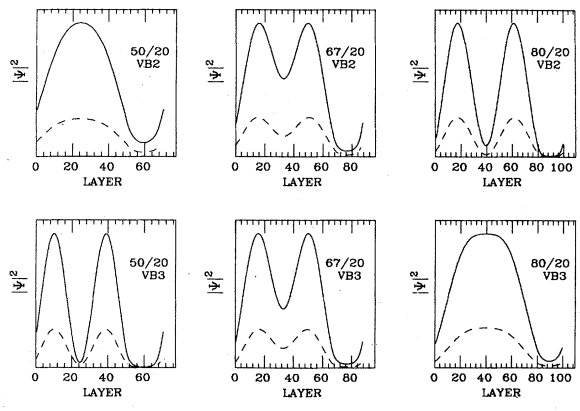

FIG. 8. Tight-binding wave functions (squared amplitudes per atomic layer) for the second (VB2) and third (VB3) valence subbands of three GaAs-$Ga_{0.7}Al_{0.3}As$ (001) superlattices with 20 alloy-barrier layers per unit cell and 50, 67, and 80 GaAs layers per unit cell. Solid line: anion. Dashed line: cation. The GaAs layers are at the left of each graph and the alloy layers are the right 20 layers.

TABLE V. Number of GaAs layers, N_c, for which the second superlattice valence subband switches from predominantly light-hole-like to predominantly heavy-hole-like. x is the barrier-alloy composition. The barrier thickness is greater than 300 Å

x	0.1	0.2	0.3	0.4	0.5	0.6	0.7	0.8	0.9	1.0
N_c	72	54	47	43	41	39	38	37	36	35

ular, superlattice optical properties are sensitive to the bulk-state composition. Reference 7 discusses the effect of band mixing on optical properties in detail.

The total amplitude squared per layer for the second (II) and third (III) valence bands are plotted in Fig. 8 for three different GaAs layer thicknesses—50, 67, and 80 atomic GaAs layers per unit cell—and 20 $Ga_{0.7}Al_{0.3}As$ layers. The solid line is for the anion and the dashed for the cation amplitudes. The left portion of each graph is for the GaAs layers and the right side (20 layers) is for the alloy barrier layers. For 50 GaAs layers, the second-band wave function is clearly an $n=1$ Kronig-Penney-type light-hole state, and the third-band wave function is an $n=2$ heavy-hole state. For 80 GaAs layers, the character of the bands can be seen to have reversed. The transitional stage is for 67 GaAs layers. Both wave functions have a double-peaked structure, but the valley between the peaks is elevated.

The GaAs layer thickness at which the crossing occurs, N_c, depends on the alloy layer thickness and on the alloy composition, x. N_c decreases with increasing alloy thicknesses, eventually reaching an asymptotic value. For any x, at most a 300-Å alloy layer thickness is needed to achieve the asymptotic value of N_c. Table V gives the values of N_c in this wide barrier limit for x values from 0.1 to 1.0. The values shown agree qualitatively with those obtained from using the Kronig-Penney model to find the layer thicknesses at which the second- and third-band Brillouin zone-center energies are the same. As an example of the effect of the alloy-barrier layer width, note that the $x=0.3$ value for N_c in Table V is 47, as compared to 67 for superlattices with 20 alloy layers discussed above.

Figure 9 summarizes the situation for finite barrier thicknesses, and alloy compositions from $x=0.2$ to 1.0. The GaAs layer thickness for which the second band becomes heavy-hole-like is plotted for the range of barrier-layer thicknesses indicated.

IV. InAs-GaSb (001) SUPERLATTICE

The bulk band structures of InAs and GaSb are shown in Fig. 10. Except for smaller effective masses, the band structures are similar to that of GaAs. As shown, the conduction-band minimum of InAs lies slightly below the valence-band maximum of GaSb. There have been various attempts to determine the magnitude of the energy difference between the two levels, E_s, both by using empirical rules and by fitting to experiment.[3,22,23] We have chosen a value of $E_s=0.10$ eV by comparing our calculated superlattice energy-band gaps with the experimental results of Refs. 22 and 24.

Since the superlattice conduction-band minimum is derived from the InAs conduction-band edge and its valence-band maximum from the GaSb heavy-hole band, the superlattice band gaps are quite sensitive to the InAs conduction-band minimum and GaSb heavy-hole-band maximum effective masses assumed.[23] Much of the variation in E_s reported can, therefore, be attributed to the variability of the assumed values of the effective masses, and not just to the difference between theoretical models. For example, White and Sham[3] assume a value of 0.431 for the GaSb heavy-hole effective mass and obtain a value of 0.175 eV for E_s. We adjust our tight-binding parameters to produce 0.33 for the same effective mass, in agreement with Refs. 4, 22, and others. This lighter mass causes the energies of our heavy-hole superlattice states to be lower (less confined). When determining E_s by fitting to the same data as White and Sham,[22] we obtain a value smaller than theirs. This is expected, since a smaller E_s brings the superlattice valence and conduction bands closer, compensating for the otherwise larger band gaps caused by the lowering of our heavy-hole superlattice energies relative to theirs.

Unfortunately, there does not seem to be precise agreement in the literature on the GaSb heavy-hole mass. In addition, there is insufficient systematic experimental data on superlattice band gaps versus layer thickness available to permit a simultaneous determination of the GaSb mass and E_s from the shape of that curve.

For large enough InAs and GaSb layer thicknesses, the superlattice undergoes a well-known semiconductor-to-semimetal transition. Charge transfer and band bending would then occur at the InAs-GaSb interfaces. In this paper we are concerned with the semiconductor regime only and therefore ignore these effects.

Table I lists the bulk InAs and GaSb band gaps and effective masses produced by the tight-binding parameters

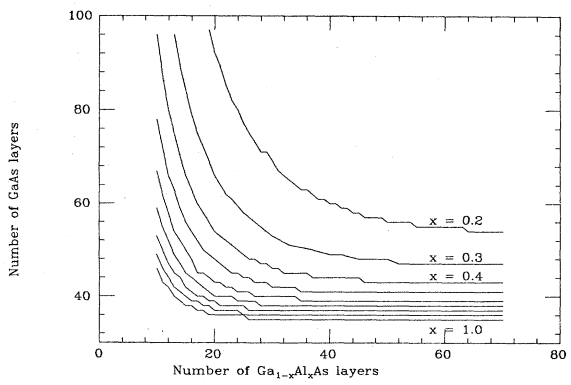

FIG. 9. Number of GaAs layers per unit cell for which the second valence subband crosses over from light-hole-like to heavy-hole-like for varying barrier thicknesses and barrier alloy compositions (x).

listed in Table II. Due to the lack of a common anion, the interface between the InAs and GaSb layers can be between either indium and antimony atoms or between gallium and arsenic atoms. The parameters for the interfaces are listed in the two columns on the right. The GaAs parameters listed there are the same as in Ref. 15. They had been determined so as to reproduce the overall GaAs density of states, whereas the GaAs parameters in the first column were adjusted to produce the bulk values shown in Table I.

Table VI illustrates the bulk composition of the superlattice states for a superlattice with 17 layers of InAs alternating with 17 layers of GaSb. One interface is chosen to be of the InSb type and the other of the GaAs type. The columns have the same meaning as in Table III. The top two zone-center states, with energies 0.977 and 0.627 eV, are conduction states, with their amplitudes mostly on the InAs layers. The lower-energy states are all in the valence band and are mostly on the GaSb layers. Note that the GaSb valence-band maximum energy is at 0.51 eV, the InAs band gap plus E_s.

Table VI contains two entries under both the "Wave vector" and the "Squared amplitude" columns for the InAs X components of the superlattice states. As can be seen in Fig. 10, there are two X-derived bulk states in InAs above approximately -0.02 eV, with wave vectors whose real parts are at the Brillouin zone boundary. Both bulk states contribute to the superlattice states as shown.

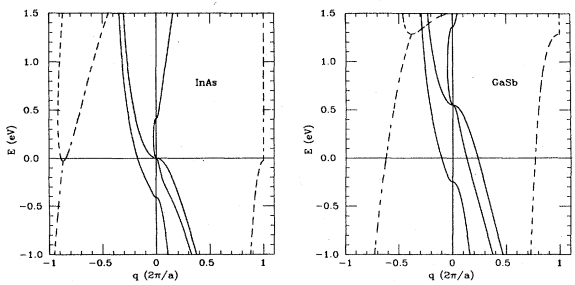

FIG. 10. Band structure of InAs (left) and GaSb (right) in the [001] direction for complex wave vector q. The zero of energy is the InAs valence-band maximum. Real q is plotted in the right portion of each graph, imaginary q in the left. The units of q are $2\pi/a$. Bands with purely real or purely imaginary q are represented by solid lines; complex q by pairs of dashed lines.

As was the case for the GaAs-AlAs superlattice states shown in Table III, most of the InAs-GaSb superlattice states are clearly identifiable as conduction, heavy-hole, or light-hole-like in character. The two conduction states do have significant contributions from the X-derived bulk components in the InAs and GaSb layers, especially the higher state. Due to the relatively large magnitudes of the imaginary parts of the X-derived wave vectors in the energy range of interest, their influence on the superlattice

TABLE VI. Energies of zone-center states of the InAs-GaSb (001) superlattice with 17 alternating layers of InAs and GaSb. The complex wave vectors and squared amplitudes of the bulk InAs and GaSb conduction-, light-hole-, heavy-hole-, split-off-, and X-point-derived components are shown. Energy is in eV. The InAs valence-band maximum is the zero of energy.

	Wave vector ($2\pi/a$)				Squared amplitude (10^{-3})			
Energy	C-LH	HH	SO	X	C-LH	HH	SO	X
				InAs				
0.977	(0.088,0)	(0,0.268)	(0,0.316)	(1.00,0.593)	20.9	0.3	0.8	6.0
				(1.00,0.901)				0.5
0.627	(0.043,0)	(0,0.228)	(0,0.283)	(1.00,0.677)	20.0	1.6	2.5	2.7
				(1.00,0.913)				0.2
0.487	(0.023,0)	(0,0.205)	(0,0.266)	(1.00,0.709)	0.0	31.7	3.6	0.0
				(1.00,0.915)				0.0
0.418	(0.007,0)	(0,0.192)	(0,0.256)	(1.00,0.726)	8.2	70.5	10.6	0.5
				(1.00,0.915)				0.1
0.383	(0,0.012)	(0,0.185)	(0,0.251)	(1.00,0.734)	46.0	0.7	2.9	4.7
				(1.00,0.915)				3.8
0.294	(0,0.022)	(0,0.164)	(0,0.237)	(1.00,0.755)	0.4	80.1	8.8	0.0
				(1.00,0.914)				0.1
0.142	(0,0.024)	(0,0.117)	(0,0.208)	(1.00,0.794)	8.7	47.8	20.8	0.7
				(1.00,0.907)				0.4
0.118	(0,0.023)	(0,0.107)	(0,0.203)	(1.00,0.801)	17.3	18.9	6.6	4.8
				(1.00,0.906)				4.5
				GaSb				
0.977	(0,0.048)	(0,0.178)	(0,0.264)	(0.863,0.457)	40.9	0.2	1.2	23.9
0.627	(0,0.035)	(0,0.095)	(0,0.230)	(0.816,0.527)	43.0	1.2	1.8	4.5
0.487	(0.017,0)	(0.043,0)	(0,0.211)	(0.804,0.550)	0.0	22.1	1.6	0.0
0.418	(0.036,0)	(0.088,0)	(0,0.201)	(0.798,0.561)	1.0	22.1	3.7	0.3
0.383	(0.044,0)	(0.104,0)	(0,0.195)	(0.795,0.567)	18.3	2.1	0.0	4.2
0.294	(0.061,0)	(0.137,0)	(0,0.180)	(0.789,0.580)	0.4	24.1	4.9	0.1
0.142	(0.089,0)	(0.184,0)	(0,0.150)	(0.779,0.601)	6.2	17.1	3.7	1.3
0.118	(0.094,0)	(0.191,0)	(0,0.144)	(0.778,0.604)	13.9	7.4	1.7	3.7

TABLE VII. Comparison of zone-center InAs-GaSb (001) superlattice state energies as calculated by the tight-binding (TB), envelope-function approximation (EF), and one-band Kronig-Penney (KP) models. The superlattice consists of 17 alternating layers of InAs and GaSb. Energies are in eV. All energies are well energies and are given relative to the edges of their respective wells.

Conduction			Heavy hole		Light hole		
KP	EF	TB	KP	TB	KP	EF	TB
0.202	0.224	0.217	−0.029	−0.023	−0.137	−0.147	−0.127
0.855	0.572	0.567	−0.117	−0.092	−0.561	−0.463	−0.392
			−0.259	−0.216			
			−0.443	−0.368			

wave functions are confined near the interfaces to within one atomic layer. Due to them, however, the wave function in the InAs layers does not match smoothly to that in the GaSb layers. Instead, there is a noticeable discontinuity in the tight-binding envelope function at the interface. This can be seen by plotting the wave functions with and without the X-derived bulk-state contributions set artificially to zero (not shown). Conventional envelope-function methods are not capable of duplicating this feature because the bulk band structure near the X point is omitted.[3–5] Thus the boundary conditions at the interfaces assumed by the envelope-function method may not be accurate in certain cases.

A similar phenomenon has been more extensively studied in the case of the GaAs-$Ga_{1-x}Al_xAs$ quantum well.[25] A much smaller interfacial discontinuity was found there. It is more significant for the InAs-GaAs superlattice because of the greater difference in atomic potentials between InAs and GaSb as compared with GaAs and AlAs.

The valence-band states shown in Table VI are clearly identifiable as either heavy-hole-like or light-hole-like, particularly within the GaSb (well) layers. The heavy-hole states have energies 0.487, 0.418, 0.294, and 0.142 eV. The light-hole states are at 0.383 and 0.118 eV. The states are not pure, however. The 0.118-eV mainly light-hole superlattice state in particular has a large bulk heavy-hole component, especially in the InAs layers. The spin-orbit split-off bulk state also has a not insignificant contribution to several of the valence-band states, even though the bulk split-off band maximum is several tenths of electron volts lower in energy. The X-point-derived bulk components have small contributions to the valence-band states. Again, the bulk components with wave vectors having nonzero imaginary parts contribute mainly near the interfaces. Since the envelope-function approximation does not take into account this mixing of bulk components for superlattice Brillouin zone-center wave functions, its treatment of the boundary conditions may be inadequate here.

Table VII compares energies predicted by the one-band Kronig-Penney (KP) model, two-band envelope-function method, and tight-binding method (TB). The tight-binding energies are the same as those listed in Table VI, but are given relative to the well edges, i.e., the InAs conduction minimum for the conduction states and the GaSb valence maximum for the heavy-hole and light-hole states. The Kronig-Penney model was quite adequate for the higher-lying GaAs-AlAs heavy-hole superlattice states (Table IV), but agrees less well with the tight-binding results for the InAs-GaSb case. The envelope-function approximation, used for the light-hole and conduction states, agrees well for conduction-band states, but only qualitatively for the light-hole states. The influence of the greater InAs-GaSb potential difference as compared to the GaAs-AlAs difference can be seen here too. The greater potential difference is more effective in causing the mixing of more than one bulk state in the valence superlattice wave function than it is for the GaAs-AlAs case, thus decreasing the accuracy of the simpler models.

The InAs and GaSb bulk bands become nonparabolic away from the zone center, similarly to the GaAs and AlAs bands, as can be seen in Fig. 11. Again, the heavy-hole band is the most parabolic. An important advantage of the envelope-function method over the Kronig-Penney model is that it also produces nonparabolic bulk light-hole and conduction bands.

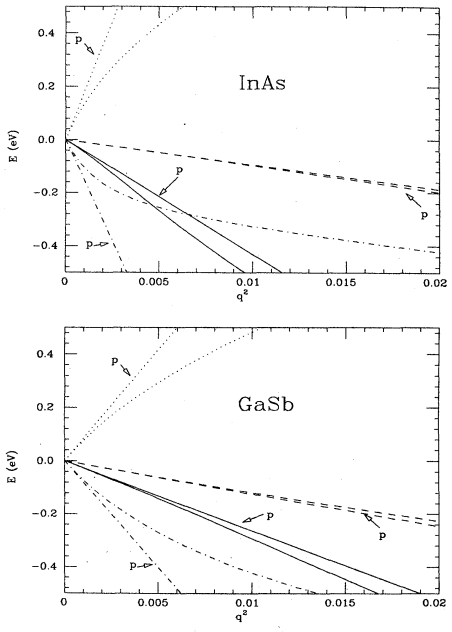

FIG. 11. Band structures of InAs (top) and GaSb (bottom) in the [001] direction versus q^2. Each band is shifted in energy so that its energy is zero at the Brillouin zone center. Dotted line: conduction band. Dashed line: heavy-hole band. Dashed-dotted line: light-hole band. Solid line: split-off band. Straight lines indicate perfectly parabolic bands (p).

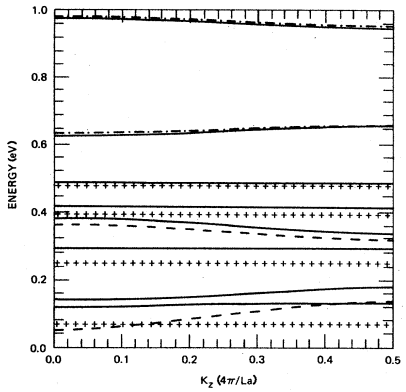

FIG. 12. InAs-GaSb (001) superlattice band structure in k_z direction for 17 InAs layers alternating with 17 GaSb layers. Solid lines: tight binding. + 's: heavy-hole Kronig-Penney model. Dashed-dotted lines: conduction-band envelope-function approximation model. Dashed lines: light-hole envelope-function approximation model. The zero of energy is the InAs valence-band maximum. L is the number of layers per unit cell, 34 in this case.

The band structure in the [001] direction for the same 17/17 InAs-GaSb superlattice is shown in Fig. 12. The solid lines are the tight-binding results. The top two curves are the two conduction bands. The envelope-function model curves are in good agreement with the tight-binding curves. The four bands indicated by plusses are the heavy-hole bands calculated with the one-band Kronig-Penney model. The topmost tight-binding valence band agrees well with the first of the effective-mass bands. The three other effective-mass heavy-hole bands are progressively lower in energy than the tight-binding bands with which they are most closely associated. Two envelope-function approximation light hole bands are indicated by dashed lines. They are also lower in energy than the associated tight-binding bands.

The dispersion in the k_x direction is shown in Fig. 13. The spin-orbit splitting is more evident here than for the GaAs-$Ga_{1-x}Al_xAs$ case shown in Fig. 5. The band mixing induced for nonzero $\mathbf{k}_t$ makes the Kronig-Penney and unmodified envelope-function methods of little use in predicting the shape of the valence subbands.

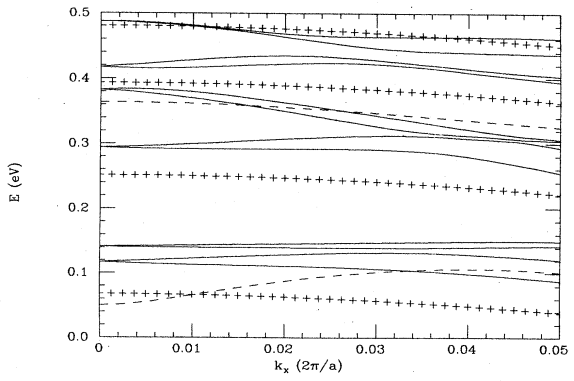

FIG. 13. InAs-GaSb (001) superlattice band structure in k_x direction for 17 InAs layers alternating with 17 GaSb layers. Solid lines: tight-binding. + 's: heavy-hole Kronig-Penney model. Dashed lines: light-hole Kronig-Penney model. The zero of energy is the InAs valence-band maximum.

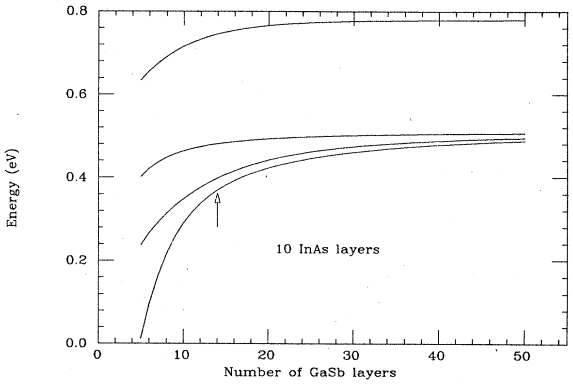

FIG. 14. Brillouin zone-center conduction- and valence-band energies for the InAs-GaSb superlattice with ten InAs layers alternating with a varying number of GaSb layers. The zero of energy is the InAs valence-band maximum. The bottommost conduction band and top three valence bands are shown. The arrow indicates the heavy-hole—light-hole crossover thickness.

The phenomenon of the crossing of bands as layer thickness is varied occurs in the InAs-GaSb superlattice in a similar manner to that for the GaAs-$Ga_{1-x}Al_xAs$ superlattice. Figure 14 shows the lowest conduction band and three highest valence-band zone-center energies for superlattices with ten InAs layers and a varying number of GaAs layers. The topmost valence band is predominantly heavy-hole-like for all layer thicknesses. The second valence band is light-hole-like for thin GaSb layer thicknesses, but becomes heavy-hole-like for more than 14 GaSb atomic double layers per GaSb slab. Plots of the light-hole and heavy-hole contents of the wave functions of these bands are similar to those in Fig. 7 for the GaAs-$Ga_{1-x}Al_xAs$ superlattice. Figure 15 plots the GaSb layer thicknesses (in numbers of GaSb atomic double layers) for which the second valence band crosses over from light-hole-like to heavy-hole-like for different InAs layer thicknesses.

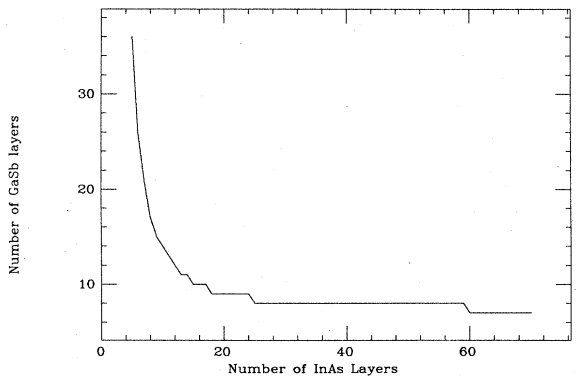

FIG. 15. Number of GaSb layers per unit cell for which the second valence subband crosses over from light-hole-like to heavy-hole-like for varying numbers of InAs layers per unit cell.

V. SUMMARY

The electronic states of semiconductor superlattices can be conveniently expressed as linear combinations of bulk states of the constituent semiconductors. In most cases for the energy ranges studied here, the zone-center superlattice states were identifiable as being predominantly composed of one type of bulk state. Admixtures of other bulk states served to modify the energies of the states somewhat and to cause wave-function discontinuities at the interfaces as compared with simpler Kronig-Penney or envelope-function approximations. More mixing was found for the InAs-GaSb superlattice as compared to the GaAs-AlAs superlattice due to the greater bulk potential differences of its constituents. For certain alloy concentrations and layer thicknesses, especially large mixing of heavy- and light-hole components occur in the second and third valence subbands. This may have a significant effect on optical-transition intensities.

The dispersion of the valence subbands in the directions parallel and perpendicular to the superlattice axis were calculated. The Kronig-Penney model for the GaAs-$Ga_{1-x}Al_xAs$ superlattice and the envelope-function approximation for the InAs-GaSb superlattice were found to give adequate agreement with the dispersion in the parallel direction for the topmost subbands, except where the crossing of subbands occurred. The multiband tight-binding method or a modified envelope-function approximation is necessary to obtain the dispersion in the perpendicular direction, where band mixing always occurs.

ACKNOWLEDGMENTS

This work was supported by U.S. Office of Naval Research Contracts Nos. N00014-82-K-0458 and N00014-81-K-0430.

---

*Present address: Hughes Research Laboratories, 3011 Malibu Canyon Road, Malibu, CA 90265.

[1]J. N. Schulman and T. C. McGill, in *Synthetic Modulated Structure Materials,* edited by L. L. Chang and B. C. Giessen (Academic, New York, 1985).

[2]J. N. Schulman and T. C. Mcgill, Phys. Rev. B **19**, 6341 (1979).

[3]S. R. White and L. J. Sham, Phys. Rev. Lett. **47**, 879 (1981).

[4]G. Bastard, Phys. Rev. B **25**, 7584 (1982).

[5]M. Altarelli, in *Proceedings of the 16th International Conference on Physics of Semiconductors, Montpellier, 1982,* edited by M. Alverous (North-Holland, Amsterdam, 1983), p. 747; Phys. Rev. B **28**, 842 (1983).

[6]J. N. Schulman and Y.-C. Chang, Phys. Rev. B **24**, 4445 (1981).

[7]Y.-C. Chang and J. N. Schulman, Appl. Phys. Lett. **43**, 536 (1983); following paper, Phys. Rev. B **31**, 2069 (1985).

[8]Optical properties of the HgTe-CdTe superlattice will be discussed in a future paper.

[9]J. N. Schulman and T. C. McGill, J. Vac. Sci. Technol. **16**, 1513 (1979).

[10]G. C. Osbourn and D. L. Smith, Phys. Rev. B **19**, 2124 (1979).

[11]Y.-C. Chang, Phys. Rev. B **25**, 605 (1982).

[12]See, G. Bastard, in *Proceedings of the NATO School on MBE and Heterostructures, Erice, Sicily, 1983,* edited by L. L. Chang (Nijhoff, The Netherlands, in press) for a thorough discussion of the envelope-function method.

[13]F. Bassani and G. P. Parravicini, *Electronic States and Optical Transitions in Solids* (Pergamon, New York, 1975), p. 116.

[14]Y.-C. Chang and J. N. Schulman, J. Vac. Sci. Technol. **21**, 540 (1982); J. N. Schulman and Y.-C. Chang, Phys. Rev. B **27**, 2346 (1983).

[15]P. Vogl, H. P. Hjalmarson, and J. D. Dow, J. Phys. Chem. Solids **44**, 365 (1983).

[16]D. H. Lee and J. D. Joannopoulos, Phys. Rev. B **23**, 4988 (1981).

[17]R. Dingle, A. C. Gossard, and W. Wiegmann, Phys. Rev. Lett. **34**, 1327 (1975).

[18]E. I. Blount, in *Solid State Physics,* edited by F. Seitz and D. Turnbull (Academic, New York, 1962), Vol. 13, Appendix C.

[19]G. F. Koster, J. O. Dimmock, R. G. Wheeler, and H. Statz, *Properties of the Thirty-two Point Groups* (MIT Press, Cambridge, 1963).

[20]E. Caruthers and P. J. Lin-Chung, Phys. Rev. B **17**, 2705 (1978).

[21]See, for example, E. Merzbacher, *Quantum Mechanics,* 2nd ed. (Wiley, New York, 1970), pp. 105—108.

[22]G. A. Sai-Halasz, L. L. Chang, J.-M. Welter, C.-A. Chang, and L. Esaki, Solid State Commun. **27**, 935 (1978).

[23]A. Madhukar, N. V. Dandekar, and R. N. Nucho, J. Vac. Sci. Technol. **16**, 1507 (1979).

[24]L. L. Chang, G. A. Sai-Halasz, L. Esaki, and R. L. Aggarwal, J. Vac. Sci. Technol. **19**, 589 (1981).

[25]J. N. Schulman, J. Vac. Sci. Technol. B **1**, 644 (1983).

[26]J. C. Slater and G. F. Koster, Phys. Rev. **94**, 1498 (1954).

[27]D. J. Chadi, Phys. Rev. B **16**, 790 (1977).